Symbiosis

www.symbiosisonline.org
www.symbiosisonlinepublishing.com
ISSN Online: 2474-9257

Research Article | Journal of Computer Science Applications and Information Technology | Open Access

Detecting and Determining the Types of Hand Bone Fracture Using K-Means Clustering

Mohammad Badrul Alam Miah and Afroza Akter*

Department of Information and Communication Technology, Mawlana Bhashani Science and Technology University, Dhaka, Bangladesh

Received: July 31, 2018; Accepted: August 23, 2018; Published: September 20, 2018

***Corresponding author:** Afroza Akter, Department of Information And Communication Technology, Mawlana Bhashani Science and Technology University, Santosh-1902, Dhaka, Bangladesh, E-mail: afrozaaktertumpa@gmail.com*

Abstract

The purpose of the proposed system is to detect and classifying the types of human hand fingers bone fracture.

As fracture is very well known to all so at first the x-ray images has been taken from Atlanta orthopedic institute, Dallas orthopedic trauma institute, De Claire Lamacchia orthopedic institute, Oliba orthopedic institute of the Bay Area. After acquiring the images image preprocessing steps have been done by noise reduction and turning into binary images with removing unwanted portions. Then k-means clustering algorithm has been applied for clustering images into six clusters as it gives a single level of clusters from large amount of data.

Feature extraction method such as moment feature, GLCM feature, entropy, major axis length, minor axis length, eccentricity, orientation, convex area, area, filled area, equivalent diameter, solidity, extent, perimeter, mean, standard deviation, correlation coefficient, median, variance, height, width, pixel count, Euclidian distance has been used for classifying the fractures into four types using Artificial Neural Network.

Keywords: Human hand fracture x-ray images; K-means clustering; GLCM; Moment feature; ANN (Artificial Neural Network);

Introduction

Comparison to other organs hands bone is the most important part of our body. Without this human is helpless. Mostly during the rainy and the winter season when after the rain and snow falls the roads become useless for walking. Especially for children and older people it becomes dangerous [17]. Having these various kinds of accidents like other organs hands bone fracture is very common.

A hand fracture is a break in one of the bones in your hand. This includes the bones in the wrist and fingers, and those that connect the wrist to the fingers. A hand fracture may be caused by twisting or bending the hand in the wrong way. It may also be caused by a fall, a crush injury, or a sports injury. The following figure 1 is about the bones of the human hand [22].

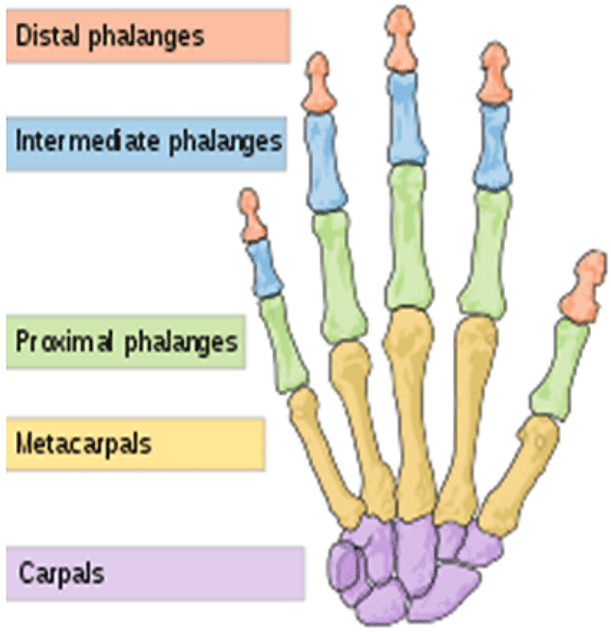

Figure 1: Bones of the human hand ["Bones in the Hand - Human Body Pictures & Diagrams - Science for Kids"]

The symbols and prefix of a finger fracture are:

- Labor or emotionalism
- Lump or pounding
- Feeling pathetic in passing one's hand
- Unusual bump or unusual shape of one's hand
- Knuckle bone looks submerged in

Types of finger fractures

i. Distal Phalanx Fractures – common type of distal fracture is tuft fracture. This fracture at the fingertip is associated with a crush injury. In the following figure 2 the arrow sign signifies the tuft fracture as the common fracture of distal phalanx fracture.

Figure 2: Radiograph of tuft fracture ["afp20120415p805-f3.jpg (275×353)"]

ii. Mallet Fracture –Mallet fractures occur at the insertion of the terminal finger. It has been caused by an axial load to the tip of an extended finger. The following figure 3 shows the fracture where the bone is fragmented at the dorsal surface of the proximal distal phalanx.

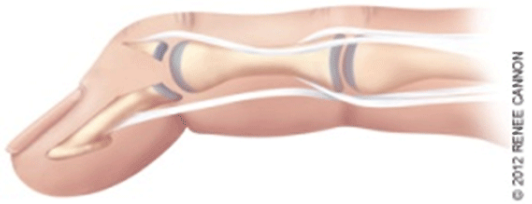

Figure 3: Mallet fracture ["afp20120415p805-f4.jpg (350×149)"]

iii. Flexor Digitorum Profundus Avulsion Fractures–An avulsion fracture causes from forced hyperextensions of a flexed DIP joint. The following figure 4 shows the fracture where the bone is fragmented at the volar surface of the proximal distal phalanx.

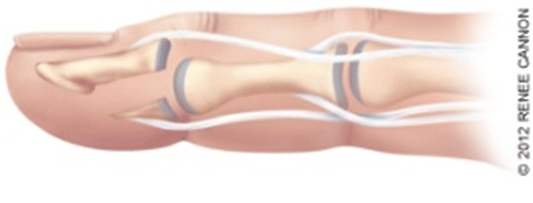

Figure 4: Flexor digitorum profundus avulsion fracture ["afp20120415p805-f5.jpg (350×120)"]

iv. Middle and Proximal Phalanx Fractures–These fractures are combined with trauma. The fractures are classified into intra or extra articular where the first is complicated and others are dislocated or located. The following figure 5 shows the proximal phalanx fracture of fingers.

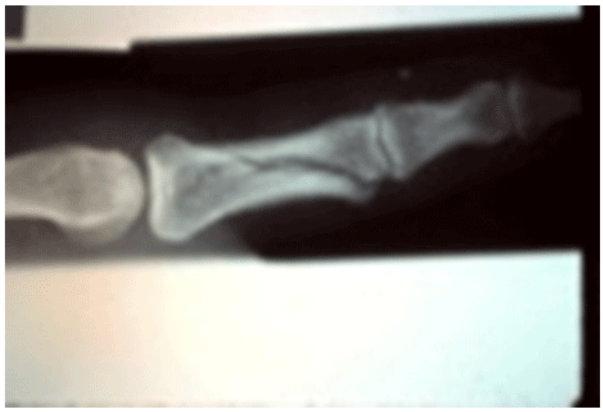

Figure 5: Proximal phalanx fracture ["Proximal Phalanx Fracture | The Hand Treatment Center - New Jersey/New York Hand Surgeon"]

Literature Review

In this section the related and the limitations of the proposed system will be discussed. Here the works is about hand fracture detection using neural network. Firstly introduce to Computer aided diagnosis which is the most effective technique for research area where the systems are used for development [18].

There are different types of medical imaging tools are available to detecting different types of problems as X-ray, Computed Tomography (CT) and Magnetic Resonance Imaging (MRI) etc. But for bone fracture detection X-ray and CT images are most frequently used. Generally doctors prefer the X-ray images to detect the fracture and where it is [15]. Though there are few limitations in X-ray but for low cost, high speed and usability it is very effective [19].

In previous, various bone fracture detection technique is introduced as Active Contour model (ACM and GACM), Wavelet and Haar, Support Vector Machine (SVM) Classifier, X-ray/CT auto classification of fracture (GLCM), Novel morphological gradient based edge detection technique and can be used segmentation or fuzzy intelligence [13,15,16,17] etc. The bone fracture is very natural in old and child ages. The normal and abnormal images have been found and it has been introduced in [20].

In [1], the GLCM (Gray Level Co-occurrence Matrix) approach has been used to segment the x-ray images of the hand and divides those separate bands [19]. After dividing the K-means clustering is used for GLCM texture analysis.

As the same way the GLCM approach has been used in [2] where it detects if the fracture in femur exists or not. Here in the preprocessing steps the images has been convert it into binary images and after applying edge detection technique the

GLCM based methods used for feature extraction and perform classification.

Another segmentation approach used for x-images of hands in [3] as bottom-up region merging method and also compute combinations between local, regional, global and hierarchical distances.

In [4], the authors proposed an adaptive interface system called AdAgen that collaborates with trained agent. Here used neural network to detect fracture in long bones and must be mentioned that their simulation result show that how NN perform detection of fracture in leg radiograph.

The most effective comparison of x-ray image segmentation techniques has been introduced in [6]. The techniques are thresholding, region-based methods, edge-based segmentation methods, clustering or cluster analysis, classification based segmentation techniques, level set methods, Active contour models, Active shape models, and Wavelet based techniques and knowledge based techniques. Among them thresholding, edge detection, classification based techniques can solve simple image segmentation problems but for complex active contour models and active shape models can be used.

On bone fracture detection there has a work [7] where fracture has been detected on measuring the neck shaft angle of the femur. On top of that [8-10] the authors suggest to use Gabor, markov random field and gradient intensity features and feed them into SVM (Support Vector Machine). They also show that these three features improve the accuracy of the model.

The system used in [11] described how the carpal bones can be extracted using automatic segmentation methods. In [12] two processes has been used for determining skeletal age. One is image preprocessing using diffusion filter and another is image segmentation using region level.

Another approaches discussed in [5,13] where authors proposed to compute the joint width in the x-ray images of hands. In [14] proposed a fusion classification technique for detecting the fracture in tibia bone in x-ray images.

Materials and Methods

In this section the proposed methods has been placed. As discussed earlier at first images has been collected then image preprocessing steps has been done, then GLCM and moment feature has been extracted then classify using ANN. The research system architecture for overall network is introduced in figure 6 as [19]: (Figure 7,8)

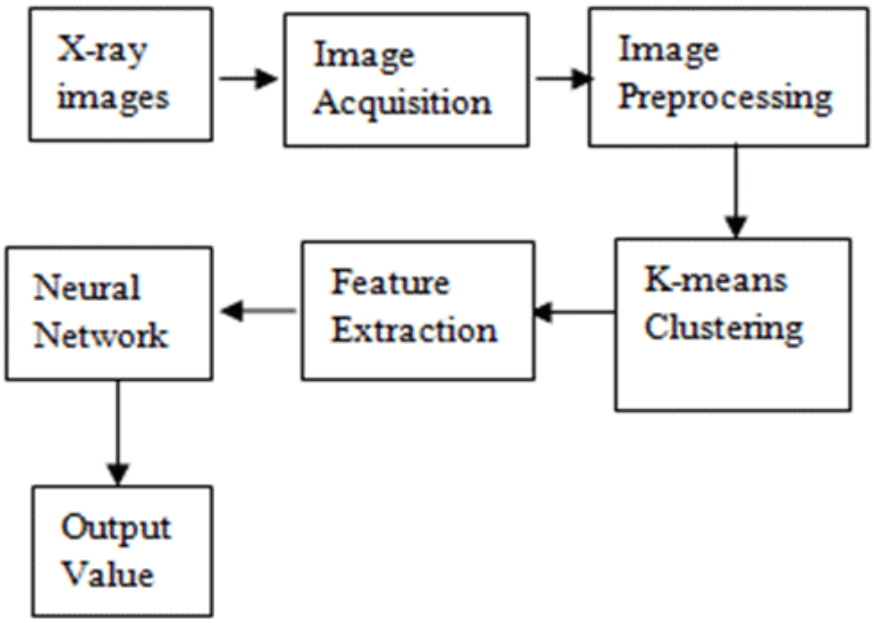

Figure 6: System architecture of detecting X-ray images

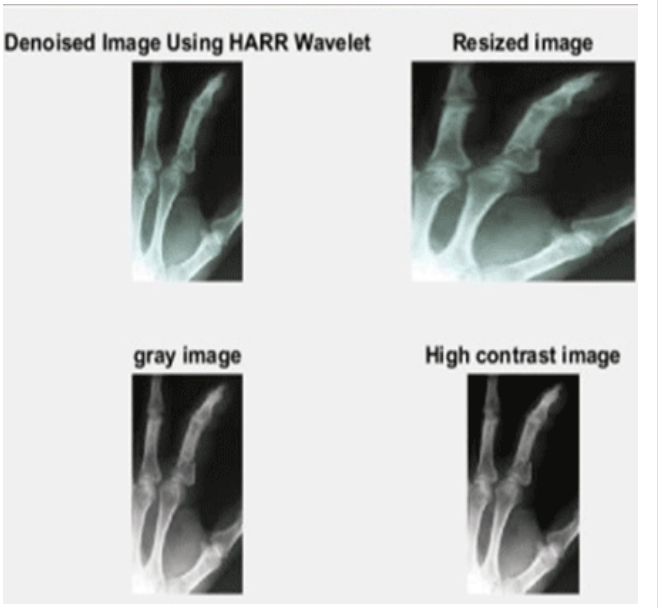

Figure 7: Image preprocessing

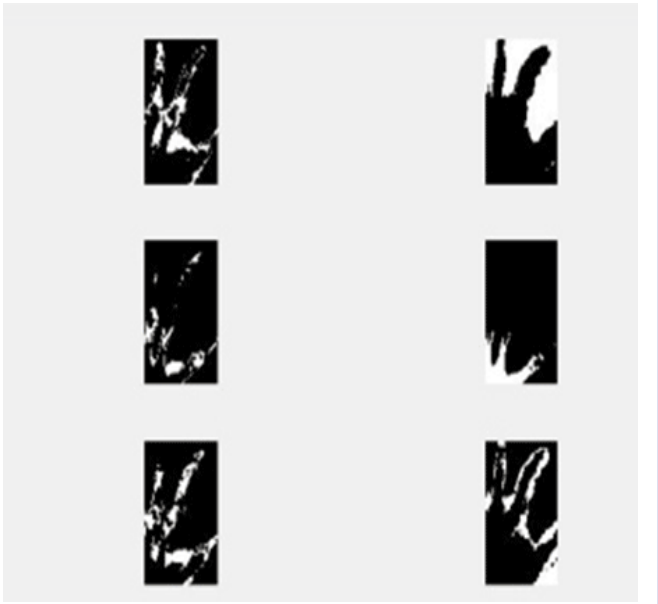

Figure 8: Performing k- means clustering

Feature Extraction

Which method is used for performing operation that can recognize the images with features is called feature extraction. It works with a large set of data or value and gives a standard combination without any difficulty. In this paper GLCM feature, Moment feature has been extracted.

a) GLCM feature extraction(1-4)

Gray Level Co-occurrence Matrix is a method for extracting the second order features. It requires a large number of matrices which provides accuracy for image estimation. It also represents the specified spatial relationship between pixels [1,2,19].

The system use GLCM to get effective texture from images.

graycomatrix function as it used to scalling and to reduce the number of intensity value in an image to eight. Where the syntax can be [21]:

glcm = *graycomatrix*(i)

But to derive several statistics form *graycoprops* function is used for providing information about the texture of an image. Where the syntax can be:

stats = *graycoprops*(glcm, properties)

stats is a structure with fields that are specified by properties.

graycoprops functions provide information as:

I. Contrast: Returns the intensity contrast between a pixel and its neighbor over the inter image.

$$Contrast = \sum_{n=0}^{G-1} n^2 \left\{ \sum_{i=1}^{G} \sum_{j=1}^{G} P(i,j) \right\}, |i-j| = n \qquad (1)$$

II. Correlation: Returns the measurement of how correlated a pixel is to its neighbor over the inter image. Range = [-1 1]; If Correlation is 1 positive relation if correlation -1 negative relation if correlation is 0 there is no relation between pixel of image.

$$Correlation = \frac{\sum_{i=0}^{N_{g-1}} \sum_{j=0}^{Ng-1} (i,j)\, p(i,j) - \mu_x \mu_y}{\sigma_x \sigma_y} \qquad (2)$$

III. Energy: Returns the sum of squared elements in the GLCM. Also known as Angular Second Moment (ASM).

$$ASM = \sum_{i=0}^{N_{g-1}} \sum_{j=0}^{N_{g-1}} P_{ij}^2 \qquad (3)$$

IV. Homogeneity: Also known as (Inverse Difference Moment) .Returns a value that measures the closeness of the distribution of elements in the GLCM to the GLCM diagonal.

$$IDM = \frac{\sum_{i=0}^{N_{g-1}} \sum_{j=0}^{N_{g-1}} P_{ij}}{1+(i-j)^2} \qquad (4)$$

b) Moment Feature Extraction(5-11)

Calculate the central moments of all orders.

SIGMA = moment(X,ORDER) returns the ORDER-th central sample moment of the values in X. For vector input, SIGMA is MEAN((X-MEAN(X))^{ORDER}).

For a matrix input, moment(X,ORDER) returns a row vector containing the central moment of each column of X. For N-D arrays, moment operates along the first non-singleton dimension. Moment(X,ORDER,DIM) takes the moment along dimension DIM of X [19,20].

The first central moment is exactly zero. The second central moment is the variance, using a divisor of N instead of N-1, where N is the sample size.

$$M_1 = \eta_{20} + \eta_{02} \quad (5)$$

$$M_2 = (\eta_{20} - \eta_{02})^2 + 4\eta_{11}^2 \quad (6)$$

$$M_3 = (\eta_{30} - 3\eta_{12})^2 + (3\eta_{21} - \eta_{03})^2 \quad (7)$$

$$M_4 = (\eta_{30} + \eta_{12})^2 + (\eta_{21} + \eta_{03})^2 \quad (8)$$

$$M_5 = (\eta_{30} - 3\eta_{12})(\eta_{30} + \eta_{12})(\eta_{30} + \eta_{12})^2 - 3(\eta_{21} + \eta_{03})^2 + (3\eta_{21} - \eta_{03})(\eta_{21} + \eta_{03})\left[3(\eta_{30} + \eta_{03})^2 - (\eta_{21} + \eta_{03})^2\right] \quad (9)$$

$$M_6 = (\eta_{20} - \eta_{20})(\eta_{30} + \eta_{12})^2 - (\eta_{21} + \eta_{03})^2 + 4\eta_{11}(\eta_{30} + \eta_{12})(\eta_{21} + \eta_{03}) \quad (10)$$

$$M_7 = (3\eta_{21} - \eta_{03})(\eta_{30} + \eta_{12})(\eta_{30} + \eta_{12})^2 - 3(\eta_{21} + \eta_{03})^2 - (\eta_{30} + 3\eta_{12})(\eta_{21} + \eta_{03})\left[3(\eta_{30} - \eta_{12})^2 - (\eta_{21} + \eta_{03})^2\right] \quad (11)$$

The seven moments are computed by normalizing central moments with order three.

c) Entropy (12)

Image entropy is the amount of information which must be coded by a compression algorithm. A perfectly flat image will have zero entropy. It has been computed as:

$$\text{Entropy} = \sum_{i=0}^{N_{g-1}} \sum_{j=0}^{N_{g-1}} -P_{ij} * LogP_{ij} \quad (12)$$

d) Major axis length (13)

Major axis length returns the length (in pixels) of the major axis of the ellipse that has the same second-moments as the region. It is calculated as following:

Major axis = a+b (13)

Where a, b are the distances from each focus to any point on the ellipse.

Minor axis length (14)

Minor axis length returns the length (in pixels) of the minor axis of the ellipse that has the same second-moments as the region. It is measured as:

$$\text{Minor axis length} = \sqrt{\left((a+b^2)+f^2\right)} \quad (14)$$

Where f is distance between focus and a, b are the distances from each focus to any point on the ellipse.

f) Eccentricity (15)

Eccentricity returns the eccentricity of the ellipse that has the same second-moments as the region. The eccentricity is the ratio of the distance between the foci of the ellipse and its major axis length. The value is between 0 and 1. (0 and 1 are degenerate cases; an ellipse whose eccentricity is 0 is actually a circle, while an ellipse whose eccentricity is 1 is a line segment.)

g) Orientation (16)

Orientation returns the angle (in degrees) between the x-axis and the major axis of the ellipse that has the same second-moments as the region.

h) Convex area (17)

Convex area returns a scalar that returns the number of pixels in convex image.

i) Area (18)

Area returns the actual number of pixels in the region. It can be calculated as:

$$D = \text{nnz}\left(1(i, j)\right) \quad (15)$$

Where nnz defines the number of nonzero matrix elements.

j) Filled area (19)

It returns the number of pixels in filled image.

k) Equiv diameter (20)

Equiv diameter returns a scalar which gives the diameter of a circle with the same area as the region. It is measured as:

$$ED = \sqrt{\frac{4*\text{Area}}{\text{pi}}} \quad (16)$$

l) Solidity (21)

It returns a scalar that gives the proportion of the pixels in the convex hull that are also in the region. It can be measured as:

$$\text{Solidity} = \frac{Area}{Convex\,area} \quad (17)$$

m) Extent (22)

Extent gives a scalar of the proportion of the pixels in the bounding box that are also in the region. It is measured as:

$$\text{Extent} = \frac{\text{Area}}{\text{Area of the bounding box}} \quad (18)$$

n) Perimeter (23)

The perimeter calculates the distance between each adjoining pair of pixels around the border of the region. If the image contains discontinuous regions, it returns unexpected results. It is measured as:

$$\text{Distance} = \sqrt{(x_2 - x_1)^2 + (y_2 - y_1)^2} \qquad (19)$$

o) Mean (24)

Mean is the average of sum of all the values in the image matrix [19,23]. It can be calculated as:

$$\text{Mean} = \text{sum}\left(\text{A}\left(\text{i}, \text{j}\right)\right) / \text{r} * c \qquad (20)$$

p) Standard Deviation (25)

Standard deviation is measures of how spread out a distribution is. The variance is computed as the average squared deviation of each number from its mean. Standard deviation is the square root of variance. It has been computed as:

$$\text{SD} = \sqrt{\text{variance}} \qquad (21)$$

a) Correlation coefficient (26)

It returns the value of correlation coefficient between two matrices or vectors of the same size.

b) Median (27)

It determines the median of the gray scale image

c) Variance (28)

This block calculates variance of the input pixels using the following equation.

$$\text{Variance} = \left(\frac{1}{M * N}\sum_{i=1}^{M}\sum_{j=1}^{N} X_{ij}^2\right)\mu^2 \qquad (22)$$

d) We also take ratio as for feature (29-30).

e) Pixel Count (31)

It gives the percentage of black pixel value of the images that has been calculated as features.

f) Euclidian Distance (32)

The Euclidean distance is commonly used for similarity measurement in image retrieval due to its efficiency. It counts the distance between two vectors of images by computing the square root of the sum of the squared absolute differences [23]. It can be calculated as follows:

$$\text{ED} = \sqrt{\sum_{k=1}^{n}(x_{1k} - x_{2k})^2} \qquad (23)$$

Result

In this section, the experimental result has been shown. At first the proposed system has been introduced as [19,20], then the following figures and tables show the results of the experiment.

Table 1: Parameter Setting

Parameter	Value
Input Layer	32
Hidden Layer	4
Output Layer	1
Learning rate	0.3

For parameter setting the following value is: Table 1

To detect hand fingers fracture images the *matlab* tool has been used as it is the high efficient language for x-ray images [21]. For classification Artificial Neural Network (ANN) with back propagation technique has been used. The system prefers this because it subtracts the training output from the target (desired answer) to obtain the error signal. It then goes BACK to adjust the weights and biases in the input and hidden layers to reduce the error.

The system used:

Training Class: 02

Targets: 0.4 for Class-1: Normal

Targets: 0.9 for Class-2: Fracture

The following figures figure 9, 10, 11, 12, 13 are the screenshot of nntraintool, performance, training state and regression of the ANN.A well trained ANN should have a very low MSE (Mean Square Error) at the end of the training phase which is measured in the figure of performance plot.

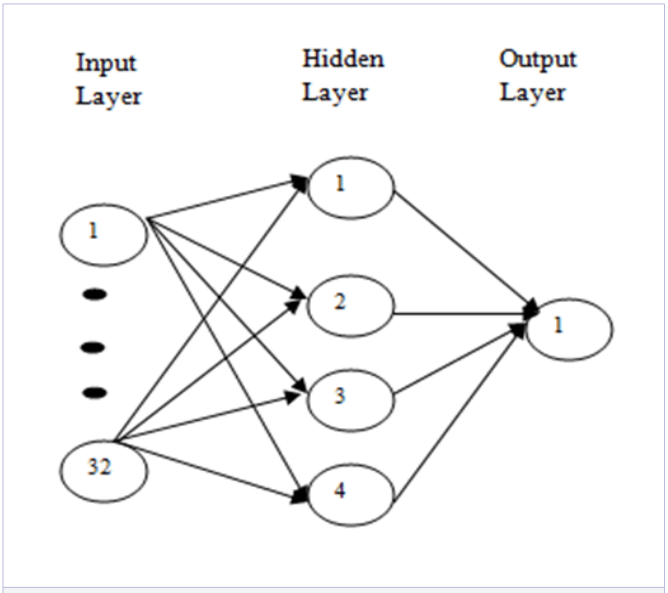

Figure 9: Proposed network design

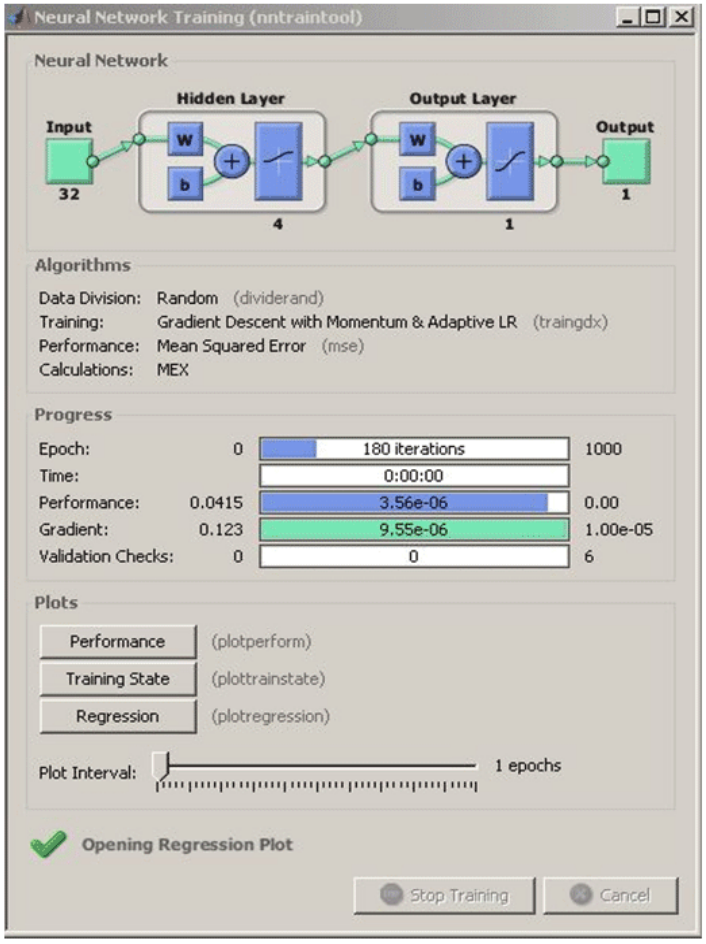

Figure 10: Training neural network

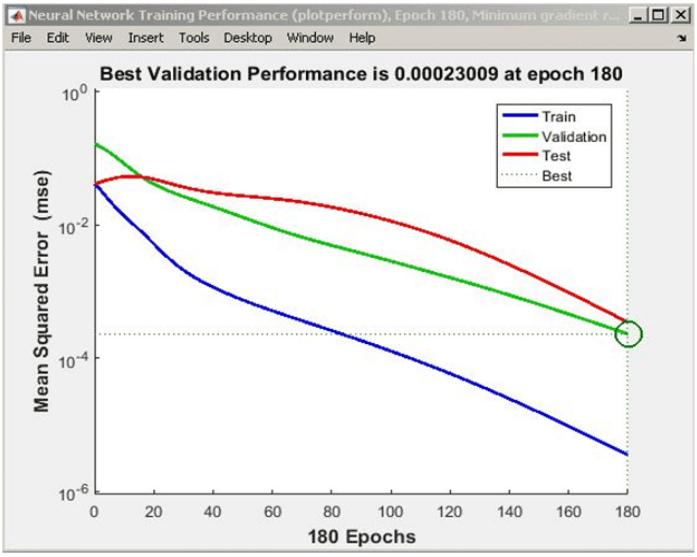

Figure 11: Performance of the Network

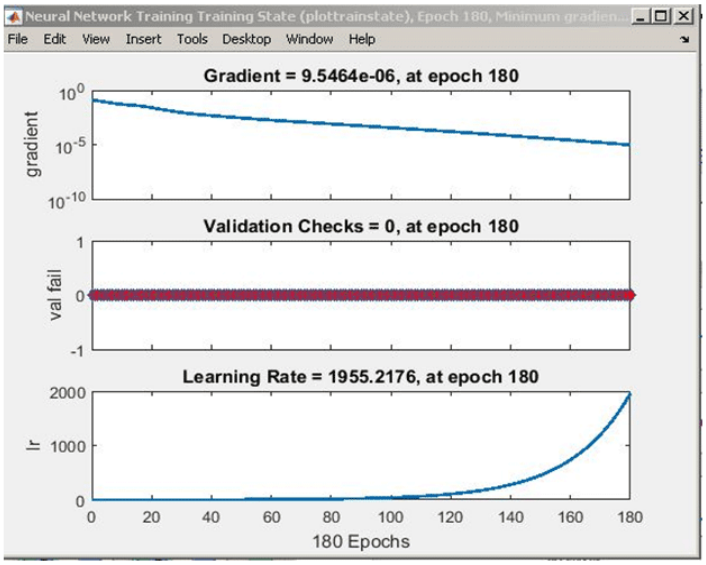

Figure 12: Training State of the network

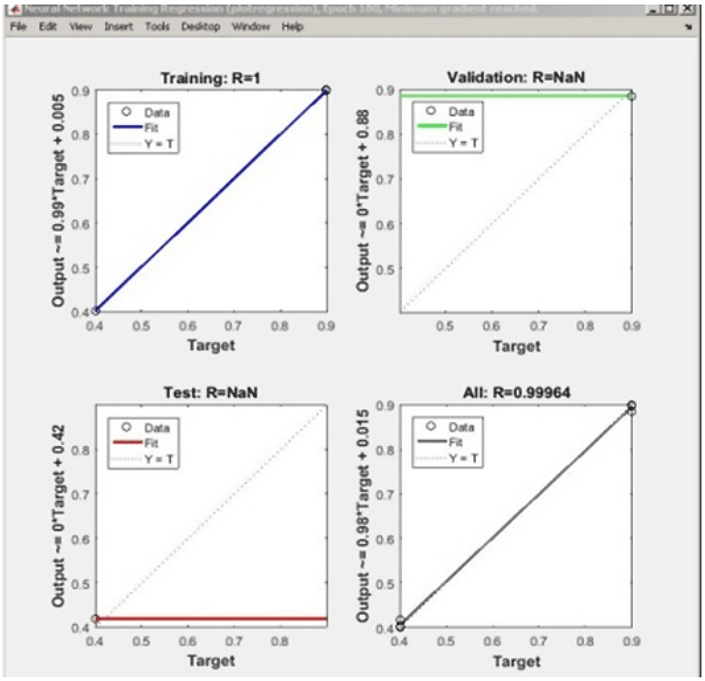

Figure 13: Regression of the network

Plotregression (targets, outputs); plots the linear regression of targets relative to outputs.

Plottrainstate (tr); plots the training state from a training record tr returned by train. (Table 2, 3, 4)

Table 2: Training with known fracture hand x-ray images

Image Type	Number of image	Correct detection	Incorrect detection	Accuracy
Group-1	25	23	2	92%
Group-2	15	14	1	93.33%
Group-3	20	17	3	85%
Total	60	54	6	90%

Table 3: Training with known normal hand x-ray images

Image	Number of image	Correct detection	Incorrect detection	Accuracy
Group-1	15	15	0	100%
Group-2	32	30	2	93.75%
Group-3	9	8	1	88.89%
Total	56	53	3	94.64%

Table 4: Compare with existing System

References	Existing System	Accuracy
[1] Al-Ayyoub M, Al-Zghool D. Determining the type of long bone fractures in x-ray images. WSEAS Transactions on Information Science and Applications. 2013;10(8);261-270.	Determining the type of long bone fractures in x-ray images	85%
[2] Al-Ayyoub M, Hmeidi I, and Rababah H. Detecting Hand Bone Fractures in X-Ray Images. JMPT. 2013;4(3);155-168.	Detecting Hand Bone Fractures in X-Ray Images	91.80%
	Proposed System	92.24%

Conclusion

In conclusion, Using SVM classifier in classification and testing phase the overall accuracy is more than 85% but using Artificial Neural Network with back propagation technique in the testing phase of this system the overall accuracy is 92.24% [18]. Though the system do not find the types of hand bone fracture but it can correctly identify if fracture exists if or not. To overcome this limitation we will work about it in future and also give the treatment of fractures.

References

1. Chai HY, Wee LK, Swee TT, Salleh SH, Ariff AK. Gray-level co-occurrence matrix bone fracture detection. American Journal of Applied Sciences. 2011;8(1):26-32.
2. Chai HY, Wee LK, Swee TT, Hussain S. GLCM based adaptive crossed reconstructed (ACR) k-mean clustering hand bone segmentation. Book GLCM based adaptive crossed reconstructed (ACR) k-mean clustering hand bone segmentation. 2011:192-197.
3. Lehmann TM, Beier D, Thies C, Seidl T. Segmentation of medical images combining local, regional, global, and hierarchical distances into a bottom-up region merging scheme. In Medical Imaging 2005: Image Processing. 2005;5747:546-556.
4. Syiam M, El-Aziem MA, El-Menshawy M. Adagen: Adaptive interface agent for x-ray fracture detection. International Journal of Computing & Information Sciences. 2004;2(3).
5. Bielecki A, Korkosz M, Zielinski B. Hand radiographs preprocessing, image representation in the finger regions and joint space width measurements for image interpretation. Pattern Recognition. 2008;41(12);3786-3798.
6. Stolojescu-CriŞan C, Holban S. A comparison of X-ray image segmentation techniques. Advances in Electrical and Computer Engineering. 2013;13(3):85-92.
7. Peng TT. Detection of Femur Fractures in X-ray images. Master of Science Thesis, National University of Singapore. 2002.
8. Lim SE, Xing Y, Chen Y, Leow WK, Howe TS, Png MA. Detection of femur and radius fractures in x-ray images. In Proc 2nd Int Conf on Advances in Medical Signal and Information. Processing. 2004;65.
9. Lum VLF, Leow WK, Chen Y, Howe TS, Png MA. Combining classifiers for bone fracture detection in X-ray images. IEEE International Conference on Image Processing. 2005. doi: 10.1109/ICIP.2005.1529959
10. Yap DWH, Chen Y, Leow WK, Howe TS, Png MA. Detecting femur fractures by texture analysis of trabeculae. Proceedings of the 17th International Conference on Pattern Recognition. 2004;3;730-733.
11. Hao S, Han Y, Zhang J, Ji Z. Automatic isolation of carpal-bone in hand x-ray medical image. Informatics and Management Science. 2013;657-662.
12. Lin P, Zheng C, Zhang F, Yang Y. X-ray carpal-bone image boundary feature analysis using region statistical feature based level set method for skeletal age assessment application. Optica Applicata. 2005;35(2).
13. Zielinski B. A fully-automated algorithm dedicated to computing metacarpophalangeal and interphalangeal joint cavity widths. Schedae Informaticae. 2007;16;47-67.
14. Mahendran SK, Baboo SS. An enhanced tibia fracture detection tool using image processing and classification fusion techniques in X-ray images. Global Journal of Computer Science and Technology. 2011;11(14);23-28.

15. Khatik I. A Study of Various Bone Fracture Detection Techniques. International Journal of Engineering and Computer Science. 2017;6(5).
16. Smith R. Segmentation and Fracture Detection in X-ray images for Traumatic Pelvic Injury. 2010.
17. Santoso H, Nakamura K. Situation Awareness Processing Based on Background and Foreground Image for Pedestrian. In SCIS & ISIS. 2006;949-954.
18. Al-Ayyoub M, Al-Zghool D. Determining the type of long bone fractures in x-ray images. WSEAS Transactions on Information Science and Applications. 2013;10(8);261-270.
19. Alam MB, Kana KA, Akter A. Detection of Brain Cancer from MRI Images using Neural Network. International Journal of Applied Information Systems. 2016;10(5):6-11.
20. Miah MBA, Yousuf MA. Detection of lung cancer from CT image using image processing and neural network. International Conference on Electrical Engineering and Information Communication Technology. 2015:1-6. doi: 10.1109/ICEEICT.2015.7307530
21. Version M. 9.0. 0 (R2016a). Math Works Inc. Natick, MA, USA. 2016.
22. Al-Ayyoub M, Hmeidi I, Rababah H. Detecting Hand Bone Fractures in X-Ray Images. JMPT. 2013;4(3);155-168.
23. Al-Amin M, Miah MBA, Mia MR. Detection of Cancerous and Non-cancerous Skin by using GLCM Matrix and Neural Network Classifier. International Journal of Computer Applications. 2015;132(8):44-49.